TOPICAL REVIEW — 2D materials: physics and device applications

Photodetecting and light-emitting devices based on two-dimensional materials*

Yuanfang Yu(于远方)[1], Feng Miao(缪峰)[2,‡], Jun He(何军)[3,§], and Zhenhua Ni(倪振华)[1,†]

[1] Department of Physics and Key Laboratory of MEMS of Ministry of Education, Southeast University, Nanjing 211189, China

[2] National Laboratory of Solid State Microstructures, School of Physics, Collaborative Innovation Center of Advanced Microstructures, Nanjing University, Nanjing 210093, China

[3] CAS Key Laboratory of Nanosystem and Hierarchical Fabrication, National Center for Nanoscience and Technology, Beijing 100190, China

(Received 23 September 2016; revised manuscript received 5 November 2016; published online 13 February 2017)

Two-dimensional (2D) materials, e.g., graphene, transition metal dichalcogenides (TMDs), and black phosphorus (BP), have demonstrated fascinating electrical and optical characteristics and exhibited great potential in optoelectronic applications. High-performance and multifunctional devices were achieved by employing diverse designs, such as hybrid systems with nanostructured materials, bulk semiconductors and organics, forming 2D heterostructures. In this review, we mainly discuss the recent progress of 2D materials in high-responsive photodetectors, light-emitting devices and single photon emitters. Hybrid systems and van der Waals heterostructure-based devices are emphasized, which exhibit great potential in state-of-the-art applications.

Keywords: two-dimensional materials, photodetector, light emission, heterostructure

PACS: 68.55.ag, 85.60.Gz, 78.60.Fi, 79.60.Jv **DOI:** 10.1088/1674-1056/26/3/036801

1. Introduction

Two-dimensional (2D) materials possess superior optical, electrical and mechanical properties and have attracted great attention in the past decade.[1–5] Graphene, as a precedent discovered character in 2D materials, has ultrahigh carrier mobility and broadband light absorption.[1,6] Charge carrier density in graphene can be effectively tuned, which enables graphene to be a promising candidate for electrically tunable devices. Different from the gapless graphene, 2D transition metal dichalcogenides (TMDs), such as MoS_2 and WSe_2, are semiconductors with bandgap ranging from 1.57 to 2 eV,[7] which are more suitable for applications such as photodetectors and light emitting diodes (LEDs). Black phosphorus (BP), a new member in the 2D materials family, exhibits direct bandgap of about ~ 1.8 and ~ 0.3 eV in its single layer and bulk form, respectively.[8–11] The bandgap of 2D semiconductors can be effectively tuned by their thickness and the properties will change accordingly, which meet the demands of various applications. Besides the 2D layered materials mentioned above, 2D non-layered materials, such as PbS and $Pb_{1-x}Sn_xSe$, also exhibit great potential in the application of optoelectronic devices. PbS has a direct narrow bandgap of ~ 0.4 eV, which is available for broad spectral detection from visible to mid-infrared region.[12,13] $Pb_{1-x}Sn_xSe$ is also a direct narrow bandgap semiconductor with great potential in infrared detection and thermoelectric conversion.[14,15] The strong light–matter interaction, broad range light absorption/emission, and high carrier mobility of 2D atomically-thin materials make them promising candidates in optoelectronic applications, such as photodetectors and light-emitting devices.

It is crucial to exploit photodetectors with high performance in terms of speed, wavelength range and sensitivity. However, high-responsive photodetection is a challenge for graphene, due to its relatively weak light absorption ($\sim 2.3\%$ per layer).[16] This problem can be solved effectively by employing hybrid architecture and the photogating mechanism, which can remarkably improve the photosensitivity by combining graphene with other nanomaterials, such as quantum dots (QDs). On the other hand, PN junction is a key construction in optoelectronic applications, such as photodetectors and LEDs. The junctions were commonly formed by chemical doping[17] and electrostatic gating.[18,19] Besides the traditional approaches, van der Waals heterostructures based on 2D materials are ideal choices for achieving state-of-the-art devices, which provides a platform for combining superiorities of different 2D layered materials, and also forming different types of junctions. In addition, single photon emitters are another important part of applications for 2D materials, which bring new opportunities to quantum technologies.

*Project supported by the National Natural Science Foundation of China (Grant Nos. 61422503 and 61376104), the Open Research Funds of Key Laboratory of MEMS of Ministry of Education of China, and the Fundamental Research Funds for the Central Universities of China.

†Corresponding author. E-mail: zhni@seu.edu.cn

‡Corresponding author. E-mail: miao@nju.edu.cn

§Corresponding author. E-mail: hej@nanoctr.cn

© 2017 Chinese Physical Society and IOP Publishing Ltd

In this review, we will discuss the recent progress on photodetecting and light-emitting applications of 2D materials. In Section 2, we mainly review a series of state-of-the-art photodetectors based on 2D materials, including graphene, TMDs, BP and 2D non-layered materials. Devices based on hybrid systems and van der Waals heterostructures are emphasized. In Section 3, the light-emitting applications of 2D materials are summarized and electroluminescence in well-designed LEDs is presented. Subsequently, single photon emission originating from the defects in 2D materials is discussed. Finally, we discuss the perspective and challenges of 2D material-based optoelectronic devices.

2. Photodetectors based on 2D materials

2.1. Mechanisms of photodetection in 2D materials

Photodetectors convert optical signals to electrical signals, which are broadly applied in communications, imaging systems and remote sensing.[20–23] Here, we simply discuss the photovoltaic and photogating effects, which are the most commonly adopted operating mechanisms for high-speed and high-responsive photodetection, respectively.

In photovoltaic detectors, the photogenerated electron–hole pairs in the channel of detectors are separated with the help of the built-in electric field at the junctions (e.g., PN junctions, Schottky junctions), thus producing photocurrent. Junctions can be formed by different approaches, for instance, by chemical doping,[17] electrostatic gating,[18,19] or combining two materials which possess different work functions.[24] Due to the ultrafast generation and separation of electron–hole pairs at the junctions, the photodetectors dominated by photovoltaic effect are capable of ultrafast photodetection.[25] In photogating devices, take graphene-based photodetectors for example, the incident light produces electron–hole pairs in photon absorbers (e.g., QDs), with one of the two types of carriers transferred to graphene and another one trapped and gated the graphene channel. Driven by bias voltage, the type of carrier transferred to graphene would recirculate between source and drain, and produce ultrahigh gain and photoresponsivity. Besides, there are other mechanisms in photodetectors, such as photo-thermoelectric effect[26,27] and bolometric effect,[28] which are not discussed here.

2.2. Hybrid photodetectors based on graphene

The ultra-broadband light absorption from ultraviolet to terahertz (THz) enables graphene to be a promising candidate for broadband photodetection. However, the responsivity of a graphene-based photodetector is limited by the relatively weak light absorption and ultrashort lifetime of photon-induced carriers. In order to meet the demands of high-responsive devices, hybrid structures with photon-absorbing materials are frequently employed.[29–31] For instance, combining QDs and graphene can effectively prolong the lifetime of photon-induced carriers and thus realizes high-responsive photodetection.[32] Hybrid phototransistors based on PbS QDs and graphene were demonstrated with ultrahigh gain and a high responsivity of $\sim 10^7$ A·W^{-1}.[32] By employing lead zirconatetitanate ($Pb(Zr_{0.2}Ti_{0.8})O_3$) (PZT) substrates instead of silicon dioxide (SiO_2), responsivity as high as 4.06×10^9 A·W^{-1} under 325 nm light illumination was achieved in a composite graphene and graphene quantum dots (GQDs) photodetector.[33] Besides QDs and graphene hybrid photodetectors, a series of novel hybrid structures have also been investigated, which will be discussed in detail below.

2.2.1. Hybrid systems with bulk semiconductors

The combination of silicon and graphene is a typical example for bulk semiconductors/graphene hybrid structure.[24,34,35] Lightly p-doped silicon was employed to form a silicon/graphene heterostructure.[34] Responsivity of such photodetector can exceed 10^4 A·W^{-1} at wavelength of 632 nm and reach 0.23 A·W^{-1} at 1550 nm. In the visible region, there are three sources of photo-induced carriers: the interband transition in graphene, the depletion region in the Schottky junction (at silicon/graphene interfaces), and the bulk region of silicon. The absorption of light by silicon can result in injection of carriers into graphene, and the large recombination timescale and the ultrafast transition of carriers within graphene lead to ultrahigh gain of the injected carriers and thereby the high responsivity of the devices. In the infrared region, graphene is the only light absorber, and the relatively smaller absorption and shorter recombination time lead to low responsivity.[34] In another silicon/graphene hybrid photodetector (Fig. 1(a)), ultrahigh quantum gain exceeds 10^6 electrons per incident photon and responsivity of nearly 10^7 A·W^{-1}were realized.[35] The quantum carrier reinvestment was proposed to explain the detailed mechanism. Excellent weak-signal detection based on silicon/graphene heterojunctions with photovoltage responsivity exceeding 10^7 V·W^{-1} was also reported.[24] The manipulation of Fermi level of graphene enables a high degree of tunability and efficient capture of photoexcited carriers. There are also other bulk semiconductors employed in graphene-based hybrid photodetectors, e.g., germanium.[36]

Besides forming silicon/graphene junctions, interfacial gating effect was also utilized to achieve high-performance photodetection. An ultra-fast and highly sensitive photodetector was achieved by employing graphene/SiO_2/lightly-doped-silicon hybrid architecture with interfacial gating mechanism (Fig. 1(b)).[37] The localized interface states at the oxide–silicon interface induce a negative depletion layer in the silicon near the interface and cause surface energy bands to

bend downwards, leading to the formation of thermal equilibrium and built-in electric field.[38] Photogenerated electron–hole pairs in silicon are separated, the holes diffusing to silicon bulk and the electrons remaining at the SiO_2/silicon interface, forming a negative voltage on the interface and thereby gating the graphene channel through capacitive coupling. The holes carrier density of graphene increased due to gating effect, and thus high photocurrent was achieved.[37] The detector exhibits superior capability on weak signal detection, with high responsivity of ~1000 A·W^{-1} for weak signal of < 1 nW (see the right graph of Fig. 1(b)). Most importantly, the response time of the device has been pushed to ~ 400 ns, due to the ultra-fast separation of electron–hole pairs at the interface.[37] Heavily doped silicon was not available due to its very short lifetime of the photogenerated electron–hole pairs, for which the negative voltage in the interface can be generally ignored.[39] The interfacial gating effect opens a new route for high responsivity in semiconductor/graphene hybrid devices.

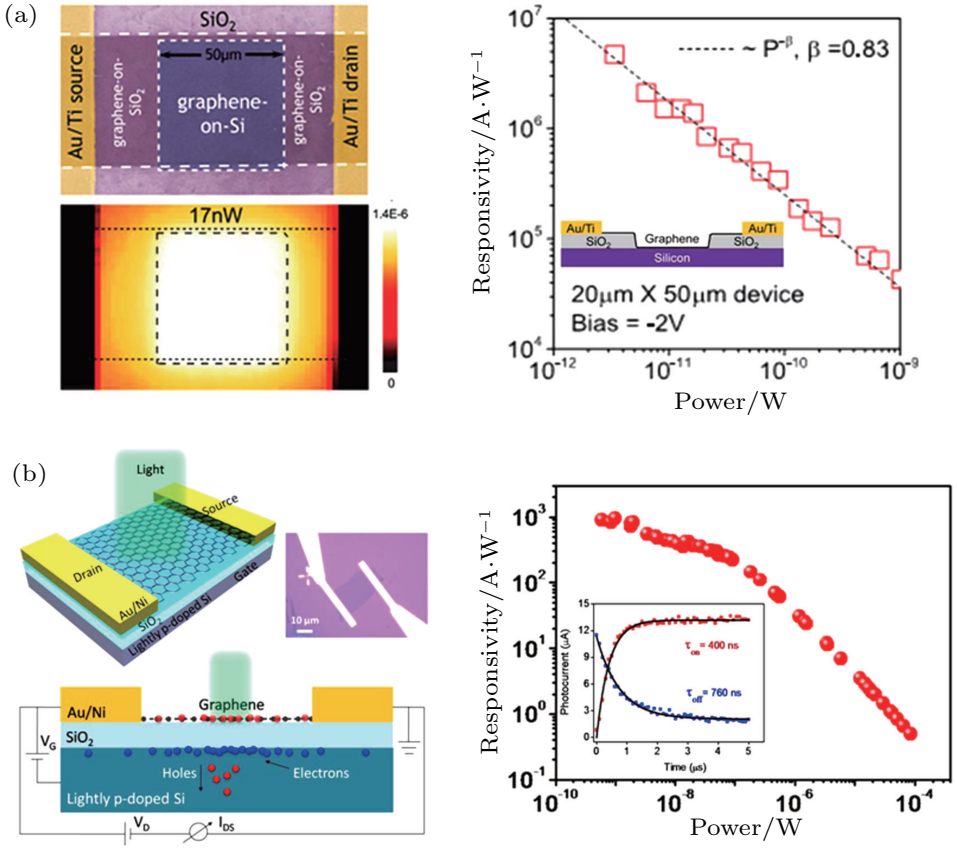


Fig. 1. (color online) (a) A pseudo-colored scanning electron microscopy (SEM) image of the silicon/graphene high-gain photodetector (top left). Photocurrent map at incident power of 17 nW shows bright photocurrent signal in the silicon/graphene region (bottom left). Photoresponsivity of the device (inset) as a function of incident power (right).[35] (b) Schematic diagram and optical image of the graphene hybrid photodetector on lightly p-doped silicon/SiO_2 substrate (left). Responsivity at $V_D = 1$ V and $V_G = 0$ V of the device as a function of the light power (right). The transient response of the device switched on or off by an acoustic optical modulator with frequency of 10 kHz. $P = \sim 0.5$ μW, $V_D = 1$ V, and $V_G = 0$ V (inset).[37]

2.2.2. Hybrid systems with organic crystals and perovskite

Except for bulk semiconductors, other light absorbing materials have also been employed in graphene-based hybrid photodetectors, such as organic crystals and organic–inorganic hybrid perovskite.[40–44] An ultrathin epitaxial organic crystal/graphene hybrid structure phototransistor is presented in Fig. 2.[40] Photogenerated electron–hole pairs in C_8-BTBT are separated by built-in electric field formed at the interface of graphene and C_8-BTBT, and electrons move toward graphene. Photoresponse of the device was studied with increasing C_8-BTBT thickness. In few-layer C_8-BTBT devices, the responsivity could reach 4.76×10^5 A·W^{-1}.[40] $CH_3NH_3P_bI_3$ perovskite/graphene hybrid system was also employed for photodetection.[41] Electrons in graphene transferred to the adjacent perovskite layer and filled the empty states in the perovskite valence band. As a result, the photoexcited electrons in the perovskite reside in the conduction band without decaying. The trapped electrons produced effective photogating effects, so that the presence of the charges altered the conductivity of the graphene channel through capacitive coupling.[45,46] The photodetector exhibits a photoresponsivity of 180 A·W^{-1} and an external quantum efficiency (EQE) of $\sim5\times10^4$% for an optical power on the microwatts scale, with photodetectivity of $\sim10^9$ Jones. There are other organic materials employed in organics/graphene hybrid photodetectors and achieved high performance, e.g., poly(3-hexylthiophene-2,5-diyl) (P3HT)[42,43] and tetraphenyl-porphyrin (H_2TPP).[44]

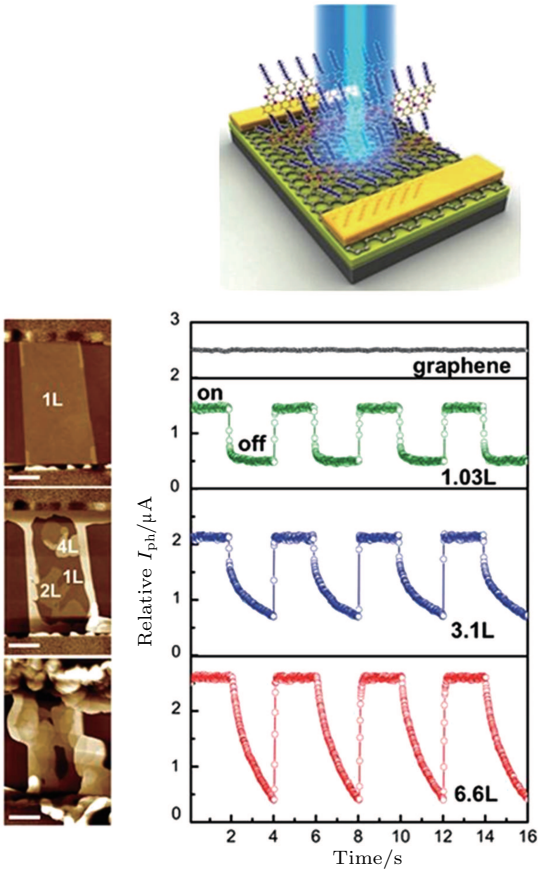


Fig. 2. (color online) Schematic of a typical organic materials/graphene hybrid phototransistor (top). Atomic force microscope (AFM) images of a device that has undergone repeated C_8-BTBT growth (bottom left). Photocurrent response of the graphene and C_8-BTBT/graphene hybrid devices under the same experimental conditions: laser power density 7000 μW·cm^{-2}, bias voltage 0.1 V, V_g–V_0 = 10 V (bottom right).[40]

2.2.3. Hybrid devices for infrared photodetection

Infrared photodetection plays an important role in the field of communications, imaging and astronomy.[20,21,47] 2D materials are easy to integrate in electronic devices, and many of them exhibit considerable photoresponse in infrared range. Hybrid architecture has been widely utilized in infrared photodetectors based on 2D materials.

Carbon nanotubes (CNTs) exhibit great potential in infrared photodetection, due to their high absorption coefficient in the infrared spectrum.[48] High detectivity up to 1.5×10^7 cm·Hz$^{1/2}$·W^{-1} has been demonstrated in a multi-wall carbon nanotube (MWCNT)/graphene hybrid photodetector, which presents a 500% improvement over the best photodetectivity achieved on MWCNT film infrared detectors.[49] Single-wall carbon nanotubes (SWCNT)/graphene hybrid film was also employed to form a large built-in potential at the interface, which performs well in the separation of electron–hole pairs and decreases the recombination of spatially isolated photocarriers.[50] The hybrid photodetector (see the inset in the top panel of Fig. 3(a)) operates in photogating mechanism and demonstrates a photoconductive gain of 10^5 with ultra-broadband sensitivity from visible to near-infrared (400–1550 nm). It exhibits great performance with a high photoresponsivity of over 100 A·W^{-1} and a fast response time of 100 μs.

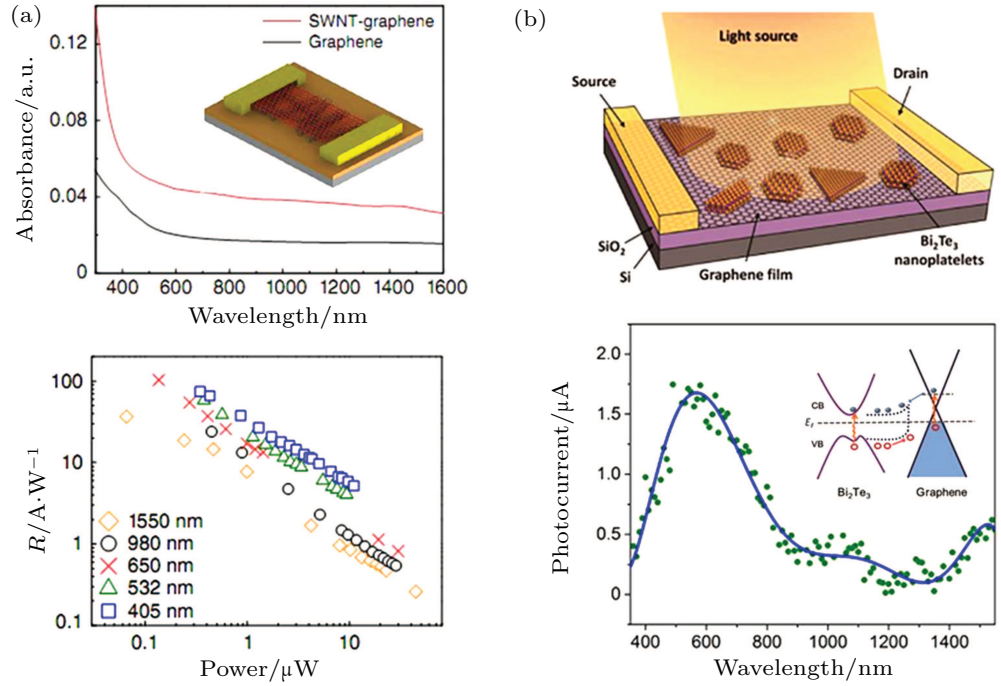


Fig. 3. (color online) (a) The ultraviolet-visible-infrared light absorbance of graphene and SWCNT/graphene hybrid film on quartz (top). Responsivities of SWCNT/graphene photodetector as a function of the optical power at different illumination wavelengths (bottom).[50] (b) Schematic of the Bi_2Te_3/graphene hybrid device (top). Photocurrent as a function of wavelength (bottom). Illustration of band structure and charge transfer (inset).[31]

Topological insulators, e.g., Bi_2Te_3, Bi_2Se_3, and Sb_2Te_3, which generally have a very small band gap (0.15–0.3 eV) in the mid-infrared range, are good candidates for infrared photodetection.[51,52] A photodetector based on Bi_2Te_3/graphene heterostructure was demonstrated (Fig. 3(b)),[31] which enables valid transfer and separation of photo-excited carriers at the Bi_2Te_3/graphene interface. Photocurrent of the device can be effectively enhanced without sacrificing the detecting spectral width. The device exhibited high responsivity from visible to infrared range (400–1550 nm, see the bottom panel of Fig. 3(b)).

Different from the hybrid photodetectors mentioned above, a broadband photodetector based on graphene double-layer heterostructure was presented, in which the photo-absorbing and electron-conductive layers are both using graphene.[53] Hot electrons and holes are separated into opposite graphene layers by selective quantum tunneling, thus hot carrier recombination was minimized. The trapped charges on the top graphene layer can lead to a strong photogating effect on the bottom graphene channel layer, yielding a considerable photoresponsivity over an ultra-broad spectral range (from visible to mid-infrared range).[53] The photoresponsivity is as high as 1.1 $A{\cdot}W^{-1}$at the wavelength of 3.2 μm. The hot carrier tunneling mechanism in the graphene double-layer heterostructure provides an available route for ultra-broadband and high-sensitivity photodetection at room temperature.[53]

2.3. Photodetectors based on TMDs and BP

2.3.1. Photodetectors based on TMDs

2D TMDs are well known for their remarkable light absorption properties, with energy gaps in the visible to the near-infrared spectral region.[54,55] High-performance photodetectors based on different types of TMDs were successfully demonstrated.[56] Single-layer MoS_2 is a direct-gap semiconductor with a bandgap of $\sim$ 1.8 eV.[57] The direct bandgap would enable efficient light absorption and electron–hole pair generation under photoexcitation. In a previous work, MoS_2 was used as the channel material in a field-effect transistor and exhibited a high channel mobility ($\sim$ 200 $cm^2{\cdot}V^{-1}{\cdot}S^{-1}$) and current ON/OFF ratio (10^8).[58] With improved mobility, as well as the contact quality and positioning technique, high-responsive monolayer MoS_2-based photodetector was realized with a maximum photoresponsivity of $\sim$880 $A{\cdot}W^{-1}$ at a wavelength of 561 nm (Fig. 4(a)).[59] Due to the short electron–hole and exciton lifetimes in MoS_2, intrinsic response times as short as 3 ps were realized in a monolayer MoS_2 photodetector (bandwidths of $\sim$ 300 GHz) (Fig. 4(b)).[60] The photo response time characterization (see the right panel of Fig. 4(b)) actually shows two distinct timescales: (i) a fast timescale of $\sim$ 4.3 ps and (ii) a slow timescale of $\sim$ 105 ps. Such phenomenon is explained by a model considering carrier capture by two different defect levels (fast and slow defects). After photoexcitation, electrons and holes in MoS_2 thermalize and lose most of their energy within a short time. Most of the photoexcited holes and then most of the electrons, are captured by the fast defects within the first few ps. Meanwhile, the minority of the holes is also captured by the slow defects.[60]

ReS_2 is another member of TMDs, which has a direct bandgap of $\sim$ 1.5 eV and exhibits anisotropic nature within the layer plane.[61] Both single and multilayer ReS_2 are direct bandgap due to the weak interlayer coupling.[62] Few layer ReS_2 has a higher density of states[63] and stronger light absorption than the thinner one.[57] Ultrahigh responsivity ($\sim$88600 $A{\cdot}W^{-1}$) phototransistors based on few-layer ReS_2 were demonstrated (see Figs. 4(c) and 4(d)), which is promising for weak signal detection.[64] The impurities or S vacancies in ReS_2 flakes act as trap states, the electrons of the photogenerated electron–hole pairs stay at the trap states for a long time and thereby present a long lifetime of holes, thus leading to the increase of the photoconductive gain. Furthermore, the use of thicker ReS_2 could increase the absorbed optical power and hence lead to large quantum efficiency.

The dark current would strongly affect the performance of photodetectors, e.g., ON/OFF ratio. Novel device architectures have been adopted in TMD-based photodetectors to suppress the dark current and improve the device performance. Ferroelectric materials combined with 2D materials have been proposed for photodetectors, with a poly(vinylidene fluoride-trifluoroethylene) (P(VDF-TrFE)) ferroelectric polymer film covered on a MoS_2 effect transistor.[65] The ferroelectric polarization could strongly suppress the dark current of the photodetector. The depleted state of carriers in the MoS_2 channel is caused by the electrostatic field derived from the remnant polarization of P(VDF-TrFE). In polarization up state, the drain-source current is the lowest compared to those of the other two states: without polarization and polarization down state. Furthermore, the band structure of few-layer MoS_2 can also be modified by the effect of the strong electric field polarization. The photoresponse wavelengths of the device were then extended from the visible to the near-infrared (0.85–1.55 μm).[65] Such ferroelectric/photoelectric 2D material hybrid system is a promising strategy for high performance 2D electronic/optoelectronic devices. In another work, gold nanoparticles (AuNPs) were employed in a WS_2 phototransistor.[66] Efficient electron trapping originating from AuNPs embedded in the gate dielectric could strongly suppress dark current. Such a device exhibited ultralow dark current (10^{-11} A), high photoresponsivity (1090 $A{\cdot}W^{-1}$) and high detectivity (3.5×10^{11} Jones) at a wavelength of 520 nm with a low bias voltage and a zero gate voltage.

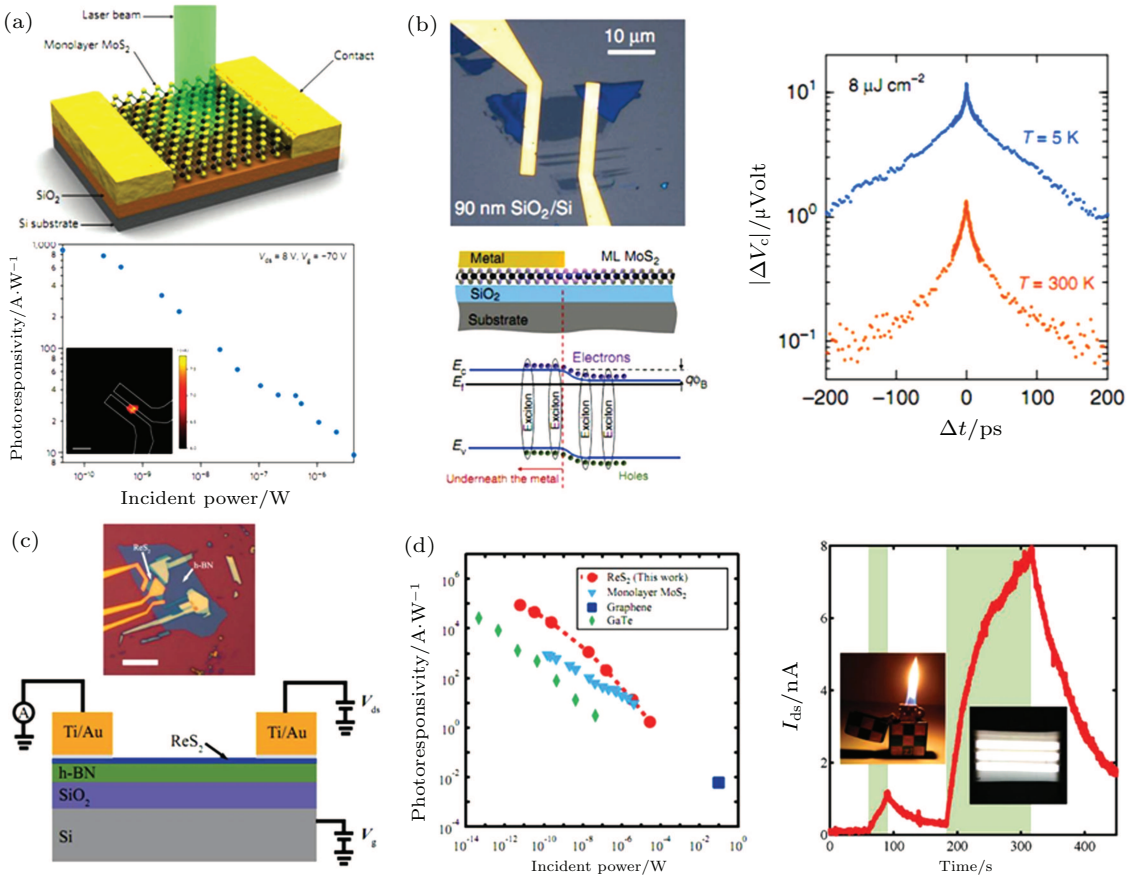


Fig. 4. (color online) (a) Cross-sectional view of the single-layer MoS_2-based photodetector under the focused laser beam (top). Photoresponsivity of the MoS_2 phototransistor (bottom). Spatial map of the photocurrent of the device (inset).[59] (b) Optical image of a back-gated monolayer MoS_2 photodetector on SiO_2/silicon substrate (top left). The energy band diagram (bottom) of the metal–MoS_2 junction (top) after photoexcitation with an optical pulse (bottom left). The photoresponse time characterization (right). The plots show two distinct timescales: a fast timescale of ~ 4.3 ps and a slow timescale of ~ 105 ps.[60] (c) Schematic and measurement circuit of the few-layer ReS_2 phototransistors.[64] (d) Photoresponsivity as a function of the incident power of few-layer ReS_2 phototransistors (left). Weak signal detection in a five-layer ReS_2 phototransistor using lighter and limited fluorescent lighting as the weak light sources (right).[64]

2.3.2. Photodetectors based on BP

As a new member in the 2D materials family, BP is an anisotropic material, which exhibits a high Hall mobility up to 1000 $cm^2 \cdot V^{-1} \cdot s^{-1}$ at room temperature.[67] BP exhibits a direct bandgap of about ~ 1.8 and ~ 0.3 eV in its single layer and bulk form, respectively,[8–11] and tunable bandgap with different thicknesses covering the visible to mid-infrared spectral range. Strong light–matter interactions in BP enable effective and efficient photoelectric conversion in photodetectors.[68,69] High responsivity of about 10^3 $A \cdot W^{-1}$ at 300 K and 7×10^6 $A \cdot W^{-1}$ at 20 K in the near-infrared region (900 nm) has been achieved in a BP-based photodetector.[70] The contact metal Ni is employed and forms a good ohmic contact to BP under p-type operation, resulting in efficient collection of the photogenerated carriers. The small contact resistance of the device greatly improves the on current and thus the photocurrent. Due to the strong intrinsic linear dichroism, BP photodetector exhibits great polarization sensitivity over a broad wavelength from 400 to 3750 nm (see Fig. 5(a)).[71] To further improve the performance, the BP flakes were patterned into an ionic gel gated electric-double-layer transistor (EDLT), which is able to tune interfacial band bending and also the Fermi level of channel materials over a large range.[72] Photogenerated electrons and holes are separated by selectively driving them into surface or bulk layers under a built-in electric field within an EDLT. Therefore, the efficiency of linear dichroism photodetector can be greatly enhanced.[71] BP was also integrated with silicon waveguide to realize high-responsive photodetection,[73] as shown in Fig. 5(b). The photocurrent was dominated by photovoltaic current at low doping case and the bolometric effect at high n-type doping case. Intrinsic responsivity reaches 135 $mA \cdot W^{-1}$ (thickness of BP 11.5 nm) and 657 $mA \cdot W^{-1}$ (thickness of BP 100 nm) at room temperature, with a high response bandwidth exceeding 3 GHz (see the right panel of Fig. 5(b)).

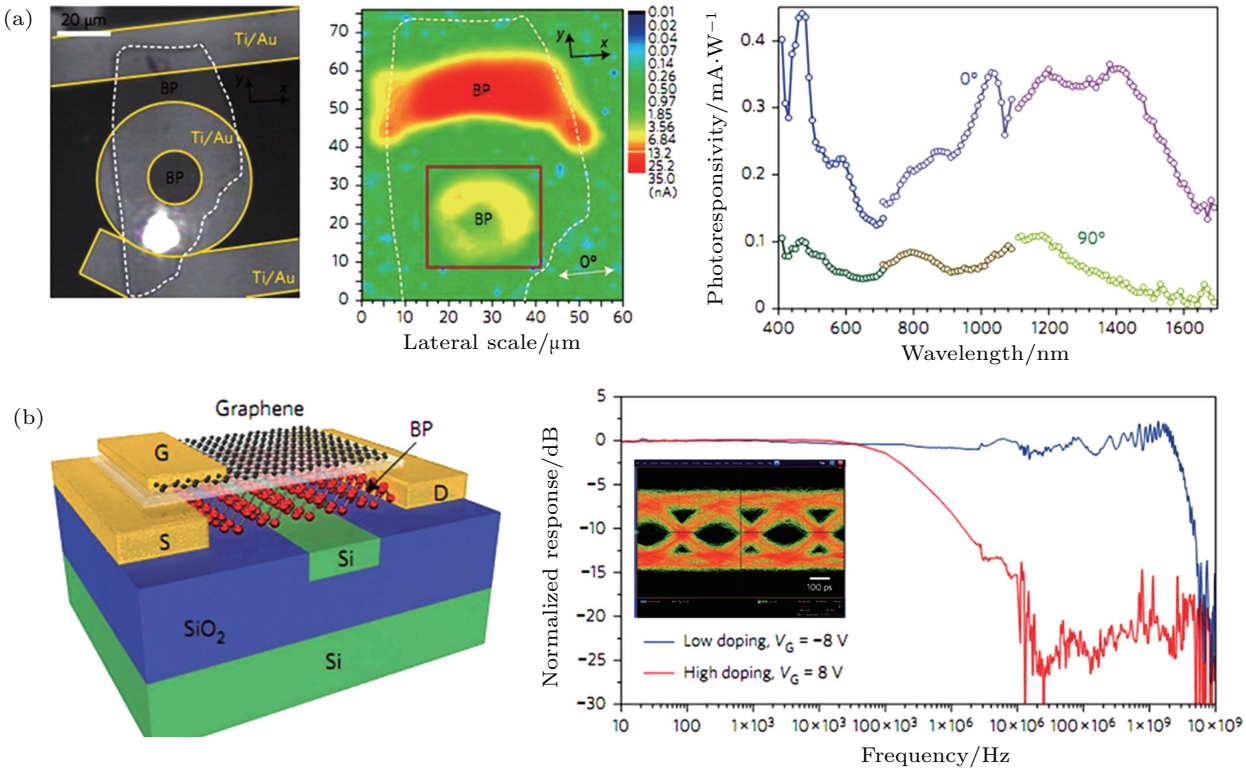


Fig. 5. (color online) (a) Optical image of a BP photodetector. Instead of a straight-edge metal electrode, the isotropic round photocurrent collector was employed to avoid the linear polarization that might arise from a straight metal edge (left). Corresponding photocurrent microscopy image of the device, with illumination at 1500 nm and polarization along the direction of the white arrow (x axis) (middle). Polarization dependence of photoresponsivity with illumination from 400 to 1700 nm, where the polarization angle of 0° corresponds to the x crystal axis and 90° corresponds to the y crystal axis (right).[71] (b) Schematic of the waveguide integrated BP photodetector (left). The response of the BP photodetector is measured when BP is gated to low and high doping conditions (right). Receiver eye diagram at a data rate of 3 GHz (inset).[73]

2.4. Photodetectors based on 2D heterostructure

Van der Waals heterostructure formed by 2D materials is commonly adopted for high performance photodetection, since it provides a platform for combining superiorities of different 2D layered materials.

Coupling graphene with MoS_2 can produce a hybrid material that combines the high photon absorption capability of MoS_2 and high carrier mobility of graphene. A photodetector based on graphene/MoS_2 heterostructure exhibits a high photogain greater than 10^8 and a photoresponsivity value higher than 10^7 A·W^{-1} (as shown in Fig. 6(a)).[74] In graphene/MoS_2 heterostructure, the electron–hole pairs are produced in the MoS_2 layer upon light illumination, and separated at the MoS_2 and graphene interfaces. The electrons can move to the graphene layer due to an effective built-in electric field, while the holes are trapped in the MoS_2 layer. The high electron mobility in graphene and the long charge-trapping lifetime of the holes leading to multiple recirculation of electrons in graphene, result in a very high photogain.[74] A photodetector based on graphene–MoS_2–graphene vertical heterostructure was also demonstrated, as shown in Fig. 6(b).[75] The amplitude and polarity of the photocurrent in the gated vertical heterostructures can be easily modulated by the electric field of an external gate, and the maximum EQE of 55% and internal quantum efficiency up to 85% was achieved. Heterostructures based on different types of TMDs are also widely investigated. The gate-tunable diode-like current rectification and a photovoltaic response across the p–n interface have been observed in p-type WSe_2 and n-type MoS_2 atomically thin vertical p–n junction, as shown in Fig. 6(c).[76] The photocurrent effectively tuned by gate voltages was shown in the bottom panel in Fig. 6(c). It was found that the interlayer tunneling recombination of the majority carriers across the van der Waals interface, which can be tuned by gating, can significantly influence both the electrical and optoelectronic properties of the junction. There are also more complicated heterostructures, e.g., a photodetector based on MoS_2–graphene–WSe_2 heterostructure, as shown in Fig. 6(d).[77] Photoexcited electrons and holes were efficiently separated by the built-in electric field formed at the depletion region of the p–n junction, and enables broadband photodetection (from the visible to infrared range) with high sensitivity. In the visible range, the photon energy is larger than the bandgaps of the TMDs materials, and abundant photogenerated free carriers are produced by all three layered materials, resulting in a considerably higher photoresponse. When the wavelength is near the infrared region and the photon energy is smaller than the bandgap of

TMDs, the interband absorption of both monolayer MoS_2 and WSe_2 is forbidden. In such case, graphene is the only photon absorbing medium, leading to a relatively smaller photoresponse of the heterostructure in the infrared range.[77] The device exhibits outstanding performance with photoresponsivity of 10^4 A·W^{-1} at 400 nm, and the specific detectivity reaches 10^{15} Jones and 10^{11} Jones in the visible and near-infrared region, respectively.[77]

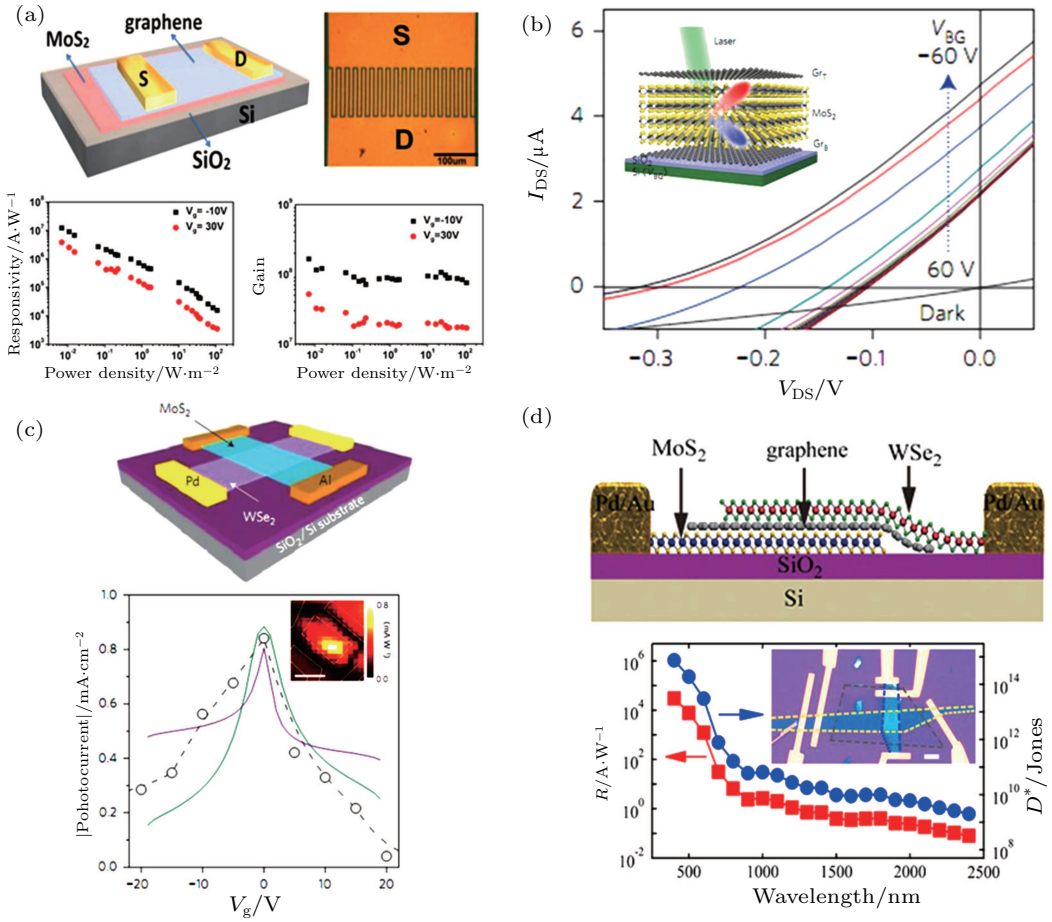


Fig. 6. (color online) (a) Schematic illustration (top left) of the photodetector based on graphene/MoS_2heterostructure, where the channel is formed in between the comb-shaped source and drain metal electrodes (top right). Photoresponsivity (bottom left) and photogain (bottom right) for the graphene/MoS_2 photodetectors.[74] (b) *I*–*V* characteristics of the graphene–MoS_2–graphene heterostructures-based device under laser illumination. Schematic illustration of the side view of the device (inset).[75] (c) Schematic diagram of a van der Waals-stacked MoS_2/WSe_2 heterojunction device with lateral metal contacts (top). Measured and simulated photocurrent at $V_{ds} = 0$ V as a function of gate voltages (bottom). Photocurrent map of the device (inset).[76] (d) Cross-section schematic of MoS_2–graphene–WSe_2 heterostructure based photodetector (top). Photoresponsivity R (left) and specific detectivity D^* (right) of a typical device for wavelengths range from 400 to 2400 nm measured in ambient air (bottom). Optical image of the device (inset).[77]

2.5. Photodetectors based on 2D non-layered materials

2D layered materials have strong lateral chemical bonding in-plane but weak van der Waals interaction between planes. On the other hand, many other materials with non-layered nature of their bulk crystals can be produced as ultrathin nanosheets and nanoplates.[78] These 2D non-layered materials, such as SnTe, $Pb_{1-x}Sn_xSe$, and $Pn_{1-x}Sn_xTe$, possess narrow bandgap and are promising candidates for infrared photodetection.[14,79–81]

$Pb_{1-x}Sn_xSe$ nanoplates with thickness from 15 to 45 nm can be fabricated from their bulk crystals, as illustrated in Fig. 7(a).[82] The crystal morphology of $Pb_{1-x}Sn_xSe$ is shown in Fig. 7(b). Flexible photodetectors based on $Pb_{1-x}Sn_xSe$ nanoplates exhibit fast, reversible, and stable photoresponse, and broad spectra detection ranging from UV to infrared. A high-performance mid-infrared detector based on $Pb_{1-x}Sn_xSe$ nanoplates with detection wavelength extending to 1.7–2.0 μm is shown in Fig. 7(c).[83] The photoresponsivity is estimated to be 318 mA·W^{-1} at the wavelength of 1.9–2.0 μm, and it shows great potential for applications in military communication, remote sensing, and environmental monitoring. PbS is a semiconductor with direct electronic bandgap of $\sim$ 0.4 eV.[12] 2D PbS nanoplates can be successfully grown by chemical vapor deposition (CVD) method, and the thickness ranges from 5 to 35 nm.[13] The devices based on 2D PbS nanoplates exhibit remarkable infrared response with high photoresponsivity (1621 A·W^{-1}), detectivity (1.72×10^{11} Jones), and photogain (2512) at the wavelength of 800 nm (see

Fig. 7(d)).[13] 2D ultrathin metal oxide nanosheets, including TiO_2, ZnO, Co_3O_4, and WO_3, are also fabricated and utilized in photodetection.[84] The metal oxide nanosheet-based devices exhibit considerable photoresponse and present excellent stability. The above results do demonstrate that photodetectors based on 2D non-layered materials exhibit excellent performance in broadband photodetection, especially in the infrared range.

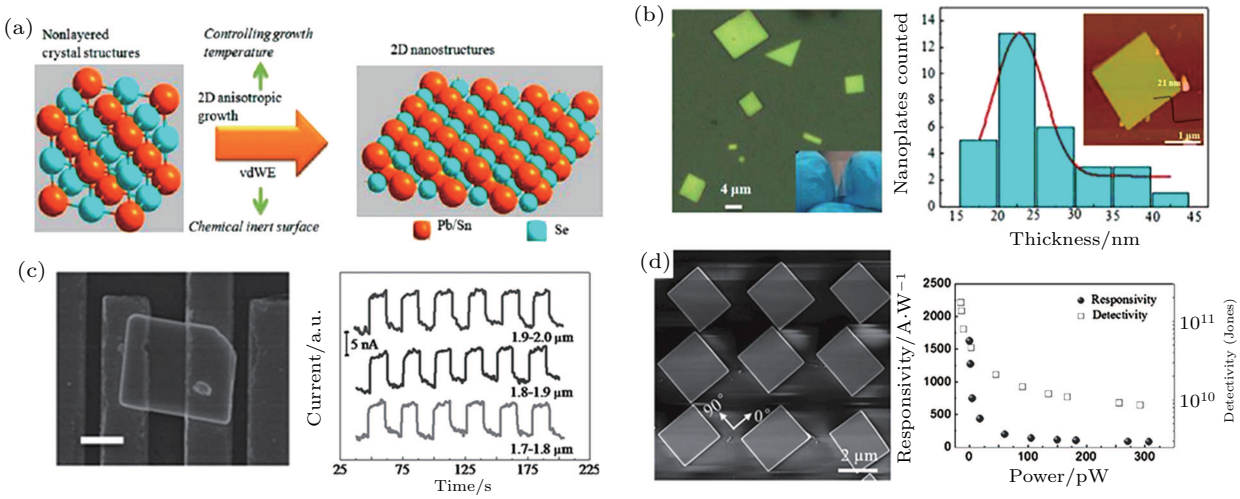


Fig. 7. (color online) (a) $Pb_{1-x}Sn_xSe$ cubic crystal structure can be tailored into ultrathin 2D nanostructure by 2D anisotropic growth.[82] (b) Optical image of $Pb_{1-x}Sn_xSe$ nanoplates (left). Histogram of $Pb_{1-x}Sn_xSe$ nanoplates thickness (right). AFM image of the nanoplate (inset).[82] (c) SEM image of the $Pb_{1-x}Sn_xSe$ nanoplate-based device (left). Mid-infrared photodetection of $Pb_{1-x}Sn_xSe$ nanoplates at 1.7–2.0 μm (right).[83] (d) SEM image of PbS nanoplate arrays (left). The photoresponsivity and detectivity of the PbS nanoplates device as a function of laser power. The wavelength of incident laser was 800 nm (right).[13]

3. Light emitting applications of 2D materials

Single-layer TMDs emerged as promising candidates for light emitting devices, which possess direct bandgap electronic band structure and high light emitting efficiency. The light emission properties are dominated by exciton effect in 2D TMDs.[85–87] Due to the strong Coulomb force interaction, charged carriers generated optically or electrically in TMDs form different kinds of combination models, such as exciton (an electron–hole pair), trion (two electrons with a hole, or two holes with an electron), or bi-exciton (two electrons with two holes).[88] In these models, exciton and bi-exciton exhibit charge-neutral, whereas trion expresses charged feature. Free excitons can also be bound within potential well, hence forming bound excitons.[89] Electroluminescence is a physical phenomenon that converts electrical energy to optical energy, which emits lights originating from the electron–hole recombination. In TMDs, p- or n-type doping can be easily realized, which benefit in constructing junctions for LEDs. In the following, we will discuss LEDs based on TMDs and heterostructures.

3.1. LEDs based on TMDs

Employing two local gates to define a p–n junction within the TMDs sheet is the most commonly used way to build LEDs.[90,91] The LEDs based on p–n junction in WSe_2 show outstanding performance with total photon emission rate up to ~ 16 million s^{-1} at applied current of 35 nA (see Fig. 8(a)).[92] In the right panel of Fig. 8(a), from left to right, the arrows indicate electroluminescence features that correspond to the impurity-bound exciton, two types of the charged excitons and the neutral exciton, respectively. Ionic-liquid gated structure is known with high gating level, and can tune the Fermi level of channel materials over a large range. Electroluminescence has also been observed in atomically thin ionic-liquid gated light-emitting transistors, as shown in Fig. 8(b).[93] Effective electron and hole accumulation in the device enables the operation of the transistors in the ambipolar injection regime, with electrons and holes injected simultaneously at the two opposite contacts of the devices, and leads to light emission. The electro- and the photoluminescence spectra are similar to each other in both the mono- and the bilayer devices (shown in the bottom right panel of Fig. 8(b)). Polarized WSe_2-based LEDs were also reported, which can emit circularly polarized electroluminescence from p–i–n junction, as shown in Fig. 8(c).[94] The circularly polarized electroluminescence is attributed to the generation of valley-polarized charge currents due to trigonal warping under high electrical bias and the valley-dependent optical selection rules. The degree of circular polarization reaches 45%, and remarkably, the polarization can be electrically controlled.

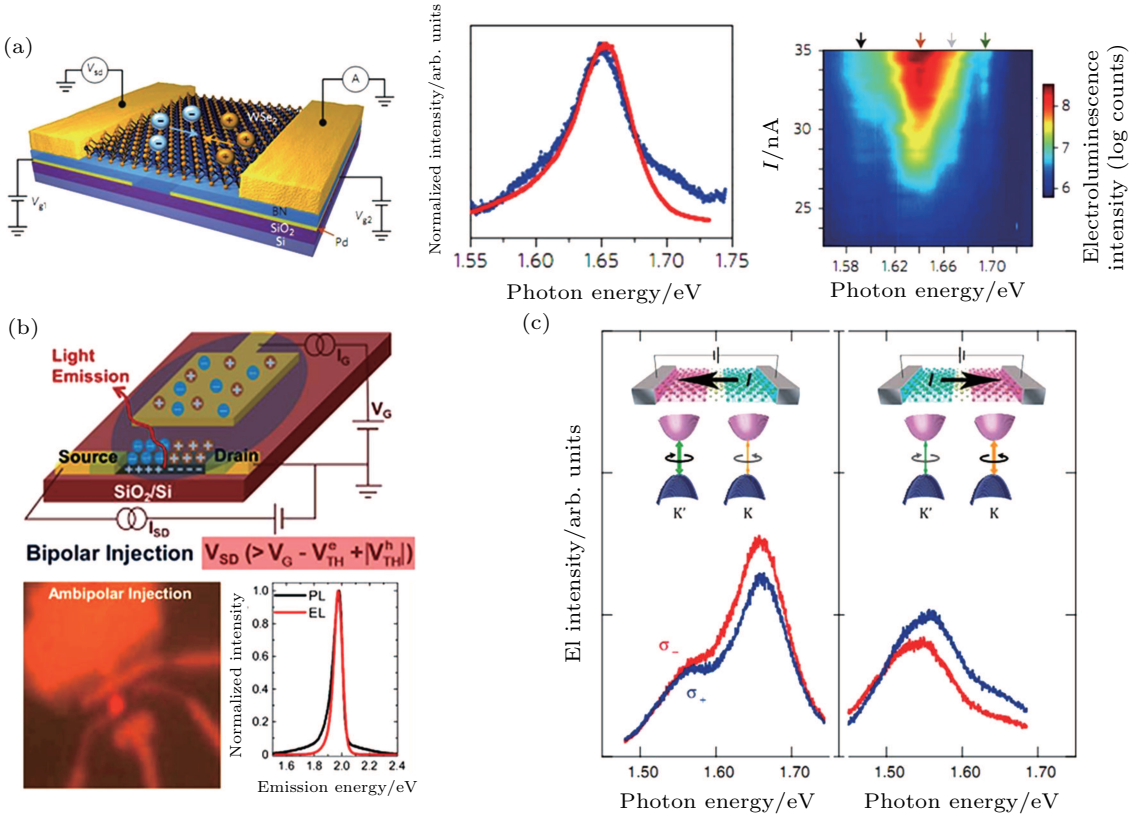


Fig. 8. (color online) (a) Schematic of monolayer WSe_2 p–n junction devices with palladium back gates (V_{g1} and V_{g2}) and source (S) and drain (D) contacts (left). Photoluminescence and electroluminescence of the LEDs (middle). Electroluminescence intensity as a function of bias current and photon energy (right). From left to right, the arrows indicate the impurity-bound exciton, the negative and positive charged excitons and the neutral exciton.[92] (b) Schematic illustrations of an ionic-liquid gated device in the ambipolar injection regime (top). Optical microscope images of the monolayer device with clearly visible spot of emitted light due to electroluminescence (bottom left). Photoluminescence and electroluminescence spectra of the LEDs (bottom right).[93] (c) Circularly polarized electroluminescence spectra from a polarized WSe_2-based LED for two opposite current directions (top). The contribution to electroluminescence from two valleys (bottom).[94]

3.2. LEDs based on heterostructure

Heterostructures based on TMDs have also been developed for LEDs. A diode of monolayer MoS_2 fabricated on a heavily p-type doped silicon substrate is shown in Fig. 9(a).[95] When a forward bias is applied to the MoS_2/silicon heterojunction, due to the direct band gap of monolayer MoS_2, the injection of holes from silicon across the junction can give rise to efficient radiative recombination. The electroluminescence spectra at room temperature and low temperature are displayed (in the bottom panel of Fig. 9(a)), two Lorentz contributions fitted in the spectra are attributed to the A exciton (labeled AX) and bound exciton (labeled DX) emission. The high signal-to-noise ratio makes it possible to identify the emission from different optical transitions. LED made with a p–i–n heterojunction of p+-Si/CVD-grown i-WS_2/n-ITO has also been reported, as shown in Fig. 9(b).[96] The heavily p-doped Si and n-ITO are adopted to inject holes and electrons into i-WS_2, respectively. The circular polarization degree of the device reaches up to 81% and can be modulated by forward current. Vertical van der Waals heterostructures have also been employed in LEDs, which enables effective charge transfer across the atomically sharp heterojunctions. WSe_2/MoS_2 heterojunction p–n diode is presented in Fig. 9(c), where the p–n junction is created over the entire WSe_2/MoS_2 overlapping area.[97] WSe_2/MoS_2 heterojunction based LEDs show prominent band edge excitonic emission and strikingly enhanced hot-electron luminescence. Such a novel heterostructure system opens up a new route to novel optoelectronic devices including atomically thin photodetectors as well as spin- or valley-polarized LEDs. Quantum wells (QW) can be formed by vertical heterostructures structure, as shown in Fig. 9(d).[98] Such vertical heterostructure-based LEDs are superior to lateral p–n junction-based devices in many aspects, including reduced contact resistance, higher current densities as well as the large luminescence area. Electrons and holes are injected into TMDs from two graphene electrodes, then recombine and emit a photon, due to the long lifetime of the quasiparticles in the QWs. The LEDs based on single quantum well present quantum efficiency above 1% and line widths of 18 meV. Furthermore, by utilizing multiple quantum wells, EQE of the device can reach 8.4%.[98]

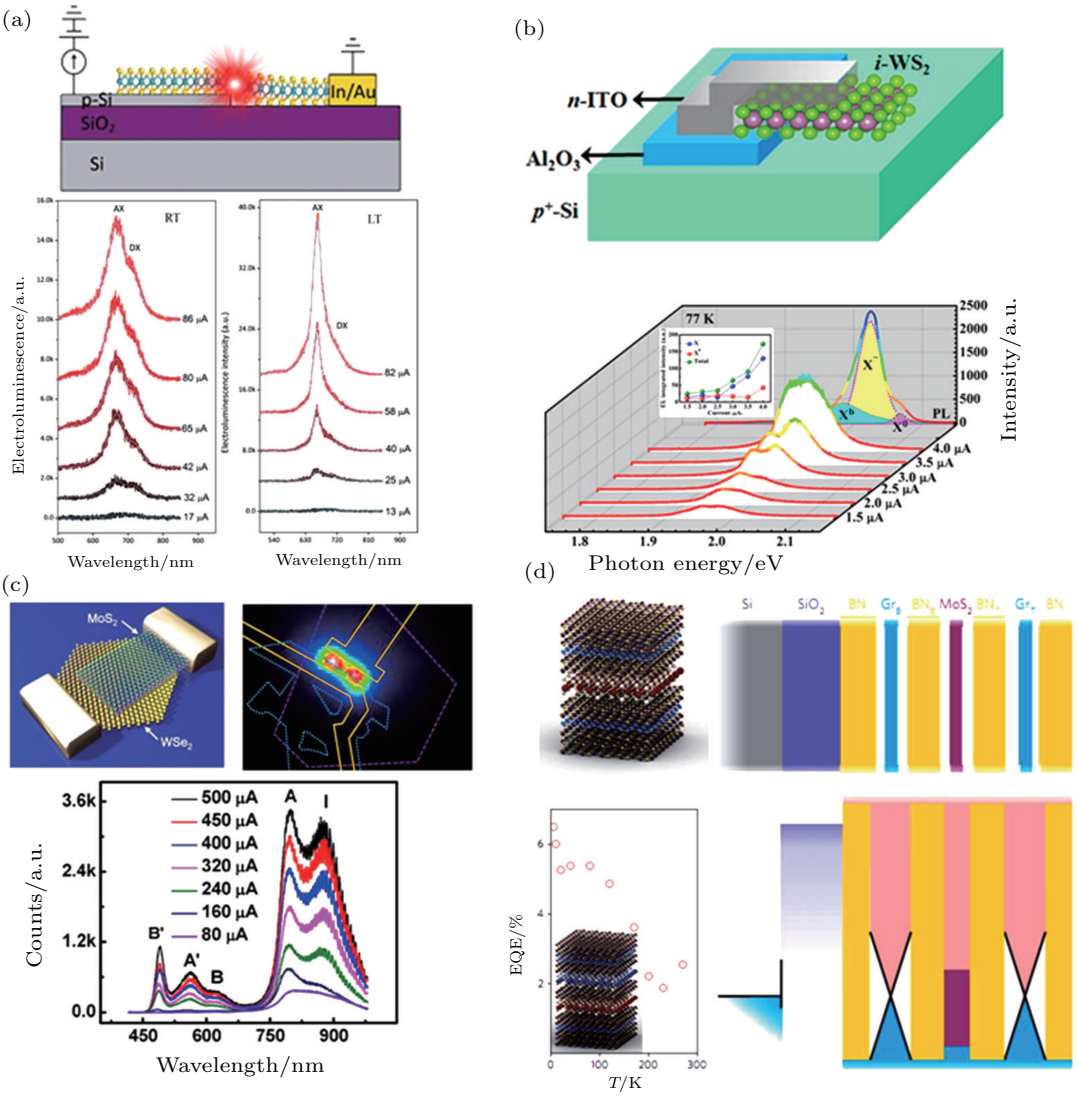


Fig. 9. (color online) (a) Schematic of the MoS_2/silicon heterojunction electroluminescence device (top). Electroluminescence spectra of a MoS_2 diode at room temperature (bottom left) and low temperature (bottom right), respectively.[95] (b) Schematic of the p+-Si/i-WS_2/n-ITO heterojunction LED device (top). Electroluminescence spectra of the LED device recorded at 77 K under different injection current (bottom).[96] (c) Schematic illustration (top left) and electroluminescence image (top right) of the WSe_2/MoS_2 heterojunction p–n diode. The electroluminescence spectra of a bilayer WSe_2/MoS_2 heterojunction at different injection current (bottom).[97] (d) Schematic of the single-quantum-well (SQW) heterostructure (top left). Schematic of the heterostructure consisting of Si/SiO_2/hBN/GrB/3hBN/MoS_2/3hBN/GrT/hBN (top right). Temperature dependence of EQE for a device with two quantum wells (QWs) made from MoS_2 and WSe_2 (bottom left). Band diagrams for the case of zero applied bias for the heterostructure are shown in the top right panel (bottom right).[98]

3.3. Single photon emitters based on 2D materials

A high-quality and high-efficiency single-photon source is required for implementing photonic quantum information processing and quantum key distribution.[99] Crystal structure imperfections can act as sources of single photon emission when they are isolated appropriately. Recently, single-photon emission from 2D materials, including WSe_2 and hexagonal boron nitride (hBN), has been reported.[100–104]

Several groups[100–103] have reported single-photon emitters in 2D WSe_2, with one of the examples shown in Fig. 10(a).[100] The emitters based on excitons spatially localized by defects in monolayer WSe_2 show very narrow linewidths of ~ 130 μeV. Through second-order correlation measurements, the strong photon antibunching is exhibited and the single-photon nature of the emission is confirmed (shown in the right panel of Fig. 10(a)). Effectively controllable single photon emission will be beneficial for quantum information processing. The single photon emission properties in WSe_2 can be controlled by external direct current electric and magnetic field manipulation (see Fig. 10(b)).[102] For example, Zeeman splitting is exhibited in many of these single photon emitters as displayed in the right panel of Fig. 10(b). Single-photon emission was also demonstrated in hexagonal boron nitride (hBN) monolayers and multilayers at room temperature,[104] which originates from a defect where a boron atom is replaced by a nitrogen atom adjacent to a vacancy. The emitters showed maximum emission rate of $I_\infty \approx 4.2 \times 10^6$ counts s^{-1} at the saturated excitation power about 611 μW, as illustrated in Fig. 10(c).

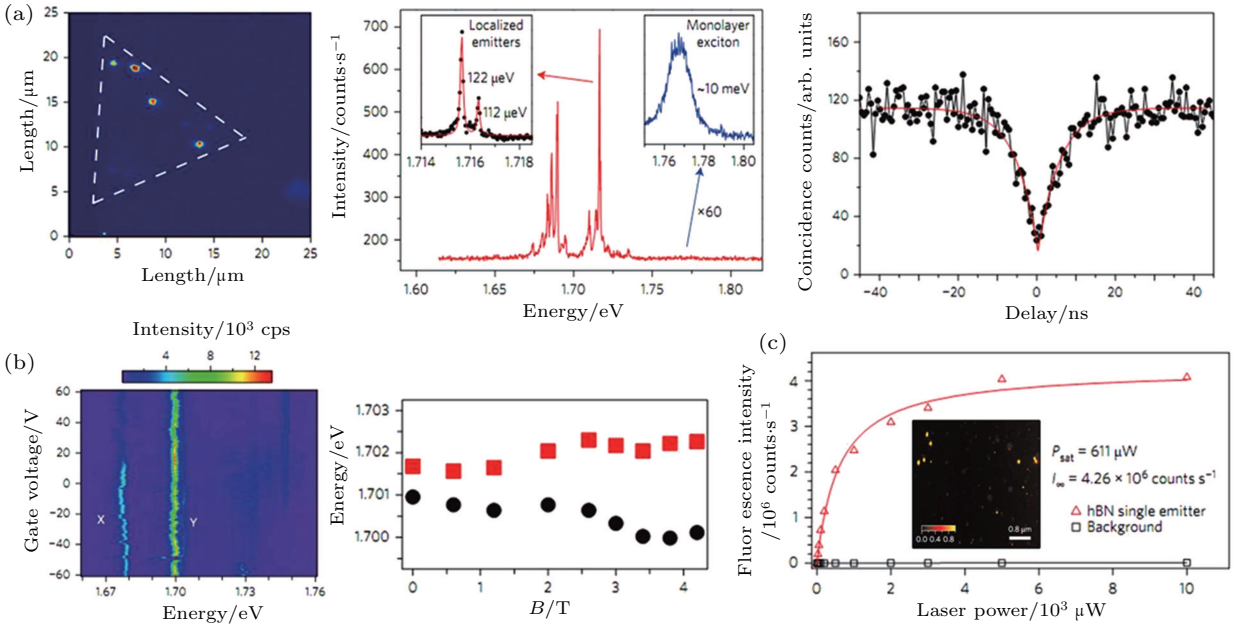


Fig. 10. (color online) (a) Photoluminescence image of isolated defect QDs in WSe_2. The dashed triangle indicates the position of the monolayer WSe_2 (left). Photoluminescence spectrum of localized emitters (middle). The emission of the localized emitters exhibits much sharper spectral lines (the linewidths of the two spectra are $\sim$ 112 and 122 μeV, respectively. left inset) than that of free excitons ($\sim$ 10 meV, right inset). Second-order correlation measurements revealed a strong photon antibunching (right).[100] (b) WSe_2 emission spectra as a function of applied gate voltage, corresponding to light emission from quantum dot-like defects (left). Magnetic field dependence of a quantum dot emission spectra in the Faraday configuration (right).[102] (c) Fluorescence saturation curve obtained from a single defect in hBN multilayers. Scanning confocal image of a multilayer hBN sample (inset).[104]

The single photon emission demonstrated in 2D material is beneficial to the development quantum technology, especially for the emitters operating at room temperature.[104] Compared with the traditional solid-state single photon emitters, which are typically embedded in bulk materials, 2D materials are easier to integrate into electronic devices and their emission properties are easier to control.

4. Outlook and perspective

In summary, great achievements have been realized in the rapidly developing field of 2D materials optoelectronics in recent years. Highly responsive graphene-based photodetectors have been realized by employing different hybrid systems, including QDs, bulk semiconductors, organics, topological insulators, and so on. TMD-based photodetectors also exhibit high performance in terms of high sensitivity and high speed, especially in the visible region. BP, as the new member of 2D materials, was extensively investigated in broadband photodetection with polarization sensitivity. Besides the 2D layered materials, 2D non-layered materials, such as SnTe, $Pb_{1-x}Sn_xSe$, and $Pn_{1-x}Sn_xTe$, possess narrow bandgaps and are promising candidates for infrared photodetection. Van der Waals heterostructures are able to combine the advantages of various 2D materials. By virtue of these constructions, strong light absorption and broadband response have been achieved. Many state-of-the-art optoelectronics, e.g., photodetectors and LEDs, are based on heterostructures. Single photon emitters have also been demonstrated in WSe_2 and hBN, with defects playing an important role inside. However, more efforts are expected on, but not restricted to, the following aspects.

i) The responsivity, dark current level, and response time are important parameters of photodetectors. High responsivity has been achieved in the photogating-effect-dominated photodetectors, but the price for achieving ultra-high sensitivity is sacrificing the response time. It is challenging to balance these parameters for specific applications.

ii) Infrared photodetection plays an important role in communications, astronomy and military systems. Besides the broadly studied layered materials, e.g., graphene and BP, the 2D non-layered materials, such as SnTe, $Pb_{1-x}Sn_xSe$, and $Pn_{1-x}Sn_xTe$, possess narrow bandgaps and are promising candidates for infrared photodetection. We expected that high-quality 2D non-layered materials would be fabricated with well-designed techniques and high-performance infrared photodetectors can further be achieved. Furthermore, hybrid system can be employed in 2D non-layered materials to enhance the light absorption and responsivity.

iii) Considerable EQE (nearly 10%) has been achieved in vertical heterostructure-based LEDs, which inspired us to explore more outstanding devices by band structure engineering in van der Waals heterostructure. It is also crucial to improve the electroluminescence efficiency by means of exploiting novel constructions and suitable materials, as well as modulating the properties of 2D materials.

iv) Defects can strongly affect the properties of 2D materials. These imperfections, such as vacancies, can act as potential resources for light emission. It demands constant effort

to achieve highly efficient LEDs and explore novel properties of different types of defects through defect engineering. It is expected that more single photon emissions originating from the defects in layered TMDs materials would be discovered in the future.

References

[1] Mak K F, Ju L, Wang F and Heinz T F 2012 *Solid State Commun.* **152** 1341
[2] Splendiani A, Sun L, Zhang Y B, Li T S, Kim J, Chim C Y, Galli G and Wang F 2010 *Nano Lett.* **10** 1271
[3] Xu X D, Yao W, Xiao D and Heinz T F 2014 *Nat. Phys.* **10** 343
[4] Castro Neto A H, Guinea F, Peres N M R, Novoselov K S and Geim A K 2009 *Rev. Mod. Phys.* **81** 109
[5] Geim A K 2009 *Science* **324** 1530
[6] Novoselov K S, Geim A K, Morozov S V, Jiang D, Zhang Y, Dubonos S V, Grigorieva I V and Firsov A A 2004 *Science* **306** 666
[7] Sun Z P, Martinez A and Wang F 2016 *Nat. Photon.* **10** 227
[8] Du Y L, Ouyang C Y, Shi S Q and Lei M S 2010 *J. Appl. Phys.* **107** 093718
[9] Akahama Y, Endo S and Narita S 1983 *J. Phys. Soc. Jpn.* **52** 2148
[10] Das S, Zhang W, Demarteau M, Hoffmann A, Dubey M and Roelofs A 2014 *Nano Lett.* **14** 5733
[11] Takao Y and Morita A 1981 *Physica B+C* **105** 93
[12] Nichols P L, Liu Z, Yin L, Turkdogan S, Fan F and Ning C Z 2015 *Nano Lett.* **15** 909
[13] Wen Y, Wang Q S, Yin L, Liu Q, Wang F, Wang F M, Wang Z X, Liu K L, Xu K, Huang Y, Shifa T A, Jiang C, Xiong J and He J 2016 *Adv. Mater.* **28** 8051
[14] Dziawa P, Kowalski B J, Dybko K, Buczko R, Szczerbakow A, Szot M, Łusakowska E, Balasubramanian T, Wojek B M, Berntsen M H, Tjernberg O and Story T 2012 *Nat. Mater.* **11** 1023
[15] Dixon J R and Hoff G F 1971 *Phys. Rev. B* **3** 4299
[16] Nair R R, Blake P, Grigorenko A N, Novoselov K S, Booth T J, Stauber T, Peres N M R and Geim A K 2008 *Science* **320** 1308
[17] Farmer D B, Golizadeh-Mojarad R, Perebeinos V, Lin Y M, Tulevski G S, Tsang J C and Avouris P 2009 *Nano Lett.* **9** 388
[18] Peters E C, Lee E J H, Burghard M and Kern K 2010 *Appl. Phys. Lett.* **97** 193102
[19] Lemme M C, Koppens F H L, Falk A L, Rudner M S, Park H, Levitov L S, and Marcus C M 2011 *Nano Lett.* **11** 4134
[20] Mueller T, Xia F N and Avouris P 2010 *Nat. Photon.* **4** 297
[21] Rogalski A, Antoszewski J and Faraone L 2009 *J. Appl. Phys.* **105** 091101
[22] Engel M, Steiner M and Avouris P 2014 *Nano Lett.* **14** 6414
[23] Chen C J, Choi K K, Chang W H and Tsui D C 1998 *Appl. Phys. Lett.* **72** 7
[24] An X H, Liu F Z, Jung Y J and Kar S 2013 *Nano Lett.* **13** 909
[25] Tielrooij K J, Piatkowski L, Massicotte M, Woessner A, Ma Q, Lee Y, Myhro K S, Lau C N, Jarillo-Herrero P, vanHulst N F and Koppens F H L 2015 *Nat. Nanotechnol.* **10** 437
[26] Wang W H, Nan H Y, Liu Q, Liang Z, Yu Z H, Liu F Y, Hu W D, Zhang W, Wang X R and Ni Z H 2015 *Appl. Phys. Lett.* **106** 021121
[27] Gabor N M, Song J C W, Ma Q, Nair N L, Taychatanapat T, Watanabe K, Taniguchi T, Levitov L S and Jarillo-Herrero P 2011 *Science* **334** 648
[28] Yan J, Kim M, Elle J A, Sushkov A B, Jenkins G S, Milchberg H M, Fuhrer M S and Drew H D 2012 *Nat. Nanotechnol.* **7** 472
[29] Klekachev A V, Cantoro M, van der Veen M H, Stesmans A L, Heyns M M and Gendt S D 2011 *Physica E* **43** 1046
[30] Guo W H, Xu S G, Wu Z F, Wang N, Loy M M T and Du S W 2013 *Small* **9** 3031
[31] Qiao H, Yuan J, Xu Z Q, Chen C Y, Lin S H, Wang Y S, Song J C, Liu Y, Khan Q, Hoh H Y, Pan C X, Li S J and Bao Q L 2015 *ACS Nano* **9** 1886
[32] Konstantatos G, Badioli M, Gaudreau L, Osmond J, Bernechea M, Arquer F P G D, Gatti F and Koppens F H L 2012 *Nat. Nanotechnol.* **7** 363
[33] Haider G, Roy P, Chiang C W, Tan W C, Liou Y R, Chang H T, Liang C T, Shih W H and Chen Y F 2016 *Adv. Funct. Mater.* **26** 620
[34] Chen Z F, Cheng Z Z, Wang J Q, Wan X, Shu C, Tsang H K, Ho H P and Xu J B 2015 *Adv. Opt. Mater.* **3** 1207
[35] Liu F Z and Kar S 2014 *ACS Nano* **8** 10270
[36] Zeng L H, Wang M Z, Hu H, Nie B, Yu Y Q, Wu C Y, Wang L, Hu J G, Xie C, Liang F X and Luo L B 2013 *ACS Appl. Mater. Interfaces* **5** 9362
[37] Guo X T, Wang W H, Nan H Y, Yu Y F, Jiang J, Zhao W W, Li J H, Zafar Z, Xiang N, Ni Z H, Hu W D, You Y M and Ni Z H 2016 *Optica* **3** 1066
[38] Schroder D K 2001 *Meas. Sci. Technol.* **12** R16
[39] Cuevas A and Macdonald D 2004 *Sol. Energ.* **76** 255
[40] Liu X L, Luo X G, Nan H Y, Guo H, Wang P, Zhang L L, Zhou M M, Yang Z Y, Shi Y, Hu W D, Ni Z H, Qiu T, Yu Z F, Xu J B and Wang X R 2016 *Adv. Mater.* **28** 5200
[41] Lee Y, Kwon J, Hwang E, Ra C H, Yoo W J, Ahn J H, Park J H and Cho J H 2015 *Adv. Mater.* **27** 41
[42] Huisman, E H, Shulga A G, Zomer P J, Tombros N, Bartesaghi D, Bisri S Z, Loi M A, Koster L J A and van Wees B J 2015 *ACS Appl. Mater. Interfaces* **7** 11083
[43] Tan W C, Shih W H and Chen Y F 2014 *Adv. Funct. Mater.* **24** 6818
[44] Kim S J, Song W, Kim S, Kang M A, Myung S, Lee S S, Lim J and An K S 2016 *Nanotechnology* **27** 075709
[45] Munoz E, Monroy E, Garrido J A, I. Izpura I, Sánchez F J, Sánchez-García M A, Calleja E, Beaumont B and Gibart P 1997 *Appl. Phys. Lett.* **71** 870
[46] Xie F, Lu H, Xiu X Q, Chen D J, Han P, Zhang R and Zheng Y D 2011 *Solid-State Electron.* **57** 39
[47] Perera A G U, Yuan H X, Choe J W and Francombe M H 1995 *SPIE's 1995 Symposium on OE/Aerospace Sensing and Dual Use Photonics*, April 17, 1995, Orlando, United States, p. 76
[48] Itkis M E, Niyogi S, Meng M E, Hamon M A, Hu H and Haddon R C 2002 *Nano Lett.* **2** 155
[49] Lu R T, Christianson C, Weintrub B and Wu J Z 2013 *ACS Appl. Mater. Interfaces* **5** 11703
[50] Liu Y D, Wang F Q, Wang X M, Wang X Z, Flahaut E, Liu X L, Li Y, Wang X R, Xu Y B, Shi Y and Zhang R 2015 *Nat. Commun.* **6** 8589
[51] Xiu F X and Zhao T T 2013 *Chin. Phys. B* **22** 96104
[52] Hasan M Z and Kane C L 2010 *Rev. Mod. Phys.* **82** 3045
[53] Liu C H, Chang Y C, Norris T B and Zhong Z H 2014 *Nat. Nanotechnol.* **9** 273
[54] Wang Q H, Kalantar-Zadeh K, Kis A, Coleman J N and Strano M S 2012 *Nat. Nanotechnol.* **7** 699
[55] Lu J P, Liu H W, Tok E S and Sow C H 2016 *Chem. Soc. Rev.* **45** 2494
[56] Lu J P, Carvalho A, Liu H W, Lim S X, Neto A H C and Sow C H 2016 *Angew. Chem. Int. Ed.* **55** 11945
[57] Mak K F, Lee C, Hone J, Shan J and Heinz T F 2010 *Phys. Rev. Lett.* **105** 136805
[58] Radisavljevic B, Radenovic A, Brivio J, Giacometti V and Kis A 2011 *Nat. Nanotechnol.* **6** 147
[59] Lopez-Sanchez O, Lembke D, Kayci M, Radenovic A and Kis A 2013 *Nat. Nanotechnol.* **8** 497
[60] Wang H N, Zhang C J, Chan W M, Tiwari S and Rana F 2015 *Nat. Commun.* **6** 8831
[61] Feng Y Q, Zhou W, Wang Y J, Zhou J, Liu E F, Fu Y J, Ni Z H, Wu X L, Yuan H T, Miao F, Wang B G, Wan X G and Xing D Y 2015 *Phys. Rev. B* **92** 054110
[62] Tongay S, Sahin H, Ko C, Luce A, Fan W, Liu K, Zhou J, Huang Y S, Ho C H, Yan J Y, Ogletree D F, Aloni S, Ji J, Li S S, Li J B, Peeters F M and Wu J Q 2014 *Nat. Commun.* **5** 3252
[63] Kim S, Konar A, Hwang W S, Lee J H, Lee J H, Yang J, Jung C, Kim H, Yoo J B, Choi J Y, Jin Y W, Lee S Y, Jena D, Choi W and Kim K 2012 *Nat. Commun.* **3** 1011
[64] Liu E F, Long M S, Zeng J W, *et al.* 2016 *Adv. Funct. Mater.* **26** 1938
[65] Wang X D, Wang P, Wang J L, Hu W D, Zhou X H, Guo N, Huang H, Sun S, Shen H, Lin T, Tang M H, Liao L, Jiang A Q, Sun J L, Meng X J, Chen X S, Lu W and Chu J H 2015 *Adv. Mater.* **27** 6575
[66] Gong F, Luo W J, Wang J L, Wang P, Fang H H, Zheng D S, Guo N, Wang J L, Luo M, Ho J C, Chen X S, Lu W, Liao L and Hu W D 2016 *Adv. Funct. Mater.* **26** 6084
[67] Xia F N, Wang H and Jia Y C 2014 *Nat. Commun.* **5** 4458
[68] Lu J P, Carvalho A, Wu J, Liu H W, Tok E S, Neto A H C, Özyilmaz B and Sow C H 2016 *Adv. Mater.* **28** 4090

[69] Lu J P, Yang J, Carvalho A, Liu H W, Lu Y R and Sow C H 2016 *Acc. Chem. Res.* **49** 1806

[70] Huang M Q, Wang M L, Chen C, Ma Z W, Li X F, Han J B and Wu Y Q 2016 *Adv. Mater.* **28** 3481

[71] Yuan H T, Liu X G, Afshinmanesh F, Li W, Xu G, Sun J, Lian B, Curto A G, Ye G J, Hikita Y, Shen Z X, Zhang S C, Chen X H, Brongersma M, Hwang H Y and Yi Cui 2015 *Nat. Nanotechnol.* **10** 707

[72] Cho J H, Lee J, Xia Y, Kim B, He Y Y, Renn M J, Lodge T P and Frisbie C D 2008 *Nat. Mater.* **7** 900

[73] Youngblood N, Chen C, Koester S J and Li M 2015 *Nat. Photon.* **9** 247

[74] Zhang W J, Chuu C P, Huang J K, Chen C H, Tsai M L, Chang Y H, Liang C T, Chen Y Z, Chueh Y L, He J H, Chou M Y and Li L J 2014 *Sci. Rep.* **4** 3826

[75] Yu W J, Liu Y, Zhou H L, Yin A X, Li Z, Huang Y and Duan X F 2013 *Nat. Nanotechnol.* **8** 952

[76] Lee C H, Lee G H, Van Der Zande A M, Chen W C, Li Y L, Han M Y, Cui X, Arefe G, Nuckolls C, Heinz T F, Guo J, Hone J and Kim P 2014 *Nat. Nanotechnol.* **9** 676

[77] Long M S, Liu E F, Wang P, *et al.* 2016 *Nano Lett.* **16** 2254

[78] Tan C L and Zhang H 2015 *Nat. Commun.* **6** 7873

[79] Hsieh T H, Lin H, Liu J W, Duan W H, Bansil A and Fu L 2012 *Nat. Commun.* **3** 982

[80] Tanaka Y, Ren Z, Sato T, Nakayama K, Souma S, Takahashi T, Segawa K and Ando Y 2012 *Nat. Phys.* **8** 800

[81] Xu S Y, Liu C, Alidoust N, et al. 2012 *Nat. Commun.* **3** 1192

[82] Wang Q S, Xu K, Wang Z X, Wang F, Huang Y, Safdar M, Zhan X Y, Wang F M, Cheng Z Z and He J 2015 *Nano Lett.* **15** 1183

[83] Wang Q S, Wen Y, Yao F R, Huang Y, Wang Z X, Li M L, Zhan X Y, Xu K, Wang F M, Wang F, Li J, Liu K H, Jiang C, Liu F Q and He J 2015 *Small* **11** 5388

[84] Sun Z Q, Liao T, Dou Y H, Hwang S M, Park M S, Jiang L, Kim J H and Dou S X 2014 *Nat. Commun.* **5** 3813

[85] Mak K F, He K L, Lee C, Lee G H, Hone J, Heinz T F and Shan J 2013 *Nat. Mater.* **12** 207

[86] Fogler M M, Butov L V and Novoselov K S 2014 *Nat. Commun.* **5** 4555

[87] Shi H Y, Yan R S, Bertolazzi S, Brivio J, Gao B, Kis A, Jena D, Xing H G and Huang L B 2013 *ACS Nano* **7** 1072

[88] Mak K F and Shan J 2016 *Nat. Photon.* **10** 216

[89] Tongay S, Suh J, Ataca C, Fan W, Luce A, Kang J S, Liu J, Ko C, Raghunathanan R, Zhou J, Ogletree F, Li J B, Grossman J C and Wu J Q 2013 *Sci. Rep.* **3** 2657

[90] Baugher B W H, Churchill H O H, Yang Y F and Jarillo-Herrero P 2014 *Nat. Nanotechnol.* **9** 262

[91] Pospischil A, Furchi M M and Mueller T 2014 *Nat. Nanotechnol.* **9** 257

[92] Ross J S, Klement P, Jones A M, Ghimire N J, Yan J Q, Mandrus D G, Taniguchi T, Watanabe K, Kitamura K, Yao W, Cobden D H and Xu X D 2014 *Nat. Nanotechnol.* **9** 268

[93] Jo S, Ubrig N, Berger H, Kuzmenko A B and Morpurgo A F 2014 *Nano Lett.* **14** 2019

[94] Zhang Y J, Oka T, Suzuki R, Ye J T and Iwasa Y 2014 *Science* **344** 725

[95] Ye Y, Ye Z L, Gharghi M, Zhu H Y, Zhao M, Wang Y, Yin X B and Zhang X 2014 *Appl. Phys. Lett.* **104** 193508

[96] Yang W H, Shang J Z, Wang J P, Shen X N, Cao B C, Peimyoo N, Zou C J, Chen Y, Wang Y L, Cong C X, Huang W and Yu T 2016 *Nano Lett.* **16** 1560

[97] Cheng R, Li D H, Zhou H L, Wang C, Yin A X, Jiang S, Liu Y, Chen Y, Huang Y and Duan X F 2014 *Nano Lett.* **14** 5590

[98] Withers F, Pozo-Zamudio O D, Mishchenko A, Rooney A P, Gholinia A, Watanabe K, Taniguchi T, Haigh S J, Geim A K, Tartakovskii A I and Novoselov K S 2015 *Nat. Mater.* **14** 301

[99] Politi A, Matthews J C F and O'Brien J L 2009 *Science* **325** 1221

[100] He Y M, Clark G, Schaibley J R, He Y, Chen M C, Wei Y J, Ding X, Zhang Q, Yao W, Xu X D, Lu C Y and Pan J W 2015 *Nat. Nanotechnol.* **10** 497

[101] Koperski, Nogajewski M K, Arora A, Cherkez V, Mallet P, Veuillen J Y, Marcus J, Kossacki P and Potemski M 2015 *Nat. Nanotechnol.* **10** 503

[102] Chakraborty C, Kinnischtzke L, Goodfellow K M, Beams R and Vamivakas A N 2015 *Nat. Nanotechnol.* **10** 507

[103] Srivastava A, Sidler M, Allain A V, Lembke D S, Kis A and Imamoğlu A 2015 *Nat. Nanotechnol.* **10** 491

[104] Tran T T, Bray K, Ford M J, Toth M and Aharonovich I 2016 *Nat. Nanotechnol.* **11** 37